PAPER

Fast snow removal algorithm based on the maximum value of the degree of polarization and angle of polarization

View the article online for updates and enhancements.

Fast snow removal algorithm based on the maximum value of the degree of polarization and angle of polarization

YongNan Lu[1,2] , MingFei Xu[1], ShuQiang Jia[1] and Wei Huang[1]

[1] State Key Laboratory of Applied Optics, Changchun Institute of Optics, Fine Mechanics and Physics, Chinese Academy of Sciences, Changchun 130033, People's Republic of China
[2] University of Chinese Academy of Sciences, Beijing 100049, People's Republic of China

E-mail: huangw@ciomp.ac.cn

Abstract

Images of outdoor scenes usually have low contrast and degraded visibility in snowy weather. Snowflakes, deemed as particles in the atmosphere, cause light scattering and absorption, blurring the images. Polarization-based scenarios are proven effective in restoring the images. However, current methods either inaccurately estimate atmospheric airlight at infinity or have low efficiency. To enhance the accuracy and efficiency for increasing visibility and correcting the color shift, we propose a simple method based on polarimetric images. This method uses the maximum value of the degree of polarization and angle of polarization by global analysis of the Stokes vector to accurately estimate atmospheric airlight at infinity and the transmission map. Experimental results confirm that this method can significantly improve the image quality without complex model implementation or any other processing and has high computational efficiency. Moreover, the comparison results demonstrate that this method can recover more details and depth information.

Keywords: image enhancement, polarimetric imaging, image reconstruction-restoration

(Some figures may appear in colour only in the online journal)

1. Introduction

The visible quality of an outdoor scene will be degraded under different conditions, such as snow, rain, haze and underwater [1–6], because of scattering and absorption of light caused by suspended particles, leading to attenuation of light irradiance received by the detector. In particular, under a dynamic weather condition, the propagation light field containing information about the scene is submerged into airlight, and it is difficult to distinguish these two types of irradiance. Furthermore, particles cause scattering of undesired light into the optical path, which results in obvious degradation of the image quality. For example, in the field of monitoring, tracking feature points will fail if the details are blurred by bad weather conditions. Meanwhile, extreme weather conditions will significantly decrease the visibility of an outdoor scene. It is difficult to capture the interesting target and extract a tiny feature under such conditions. Therefore, it is critical to improve image quality, enhance visibility in a turbid medium, and keep the color fidelity of scenes under such weather conditions.

Much research has included image restoration under extreme weather conditions to eliminate scattered light and enhance the visibility of scenes. These techniques can be classified into two categories, one is based on computer vision and the other is based on the optical method. Computer vision techniques include a filter (denoise) [7–11] and restructure a physical model [12–16]. Although these techniques have merit in reconstructing and recovering the degraded image, they always require using stronger prior knowledge or presume parameters [17], which have a larger error that leads to an unnatural restored image. Meanwhile, some schemes can only be utilized under some suitable condition, when the objects have higher brightness, even brighter than

atmospheric light, which results in inaccurate estimation of atmospheric light at infinity. Therefore, the methods of computer vision are applied in a suitable physical model, and these types of methods need rigorous physical parameters. The optical method is based on the infrared imaging method [18–20]. Although this type of method can acquire better images under the condition of bad weather, infrared devices have low resolution and a high price, so they are difficult to apply universally. Another way is the use of polarimetric images to obtain information about scene structure and atmospheric properties and reconstruct the image to enhance visibility and correct the color shift [19]. However, the polarimetric scheme mainly relies on the sky region to estimate the atmospheric scattering model of airlight [17, 21]. This means that this scenario can only be used for images with the sky region; therefore, a method without sky region usage was proposed [22]. Later on, a method that jointly considers polarization effects of both the sky region and object radiance was proposed to restore images [23]. Currently, a method that does not depend on whether the image includes the sky area was proposed [24]. However, these methods are based on more complicated formulas and need more computational cost to reconstruct the image.

Weather conditions are artificially classified into steady (haze, fog, and mist) or dynamic (snow, rain, and hail) [1]. The image quality could be severely degraded by these kinds of weather conditions. The haze-free methods to process the images are mainly in meteorological conditions of thin haze. These methods can be considered to process the snow-free image. However, in snowy weather, due to the particle diameter of snowflakes being larger than suspended particles (haze/fog), the scattering and absorbance of scenes light caused by snowflakes is stronger than suspended particles (haze/fog). Moreover, as snowy days are always overcast, it will lead the scenes to have low saturation. Therefore, it is difficult to reconstruct the image using the haze-free method.

In this study, we aim at restoring images and increasing the contrast in dynamic snow weather. Observing the scenes in a long range under this weather condition, the snowflakes can be approximately considered as suspended particles. The backscattered light and signal attenuation caused by snowflakes are severely degraded by the image quality. Even the noise pollution caused by dynamic snowflakes, which will make some detailed information, might be submerged. Therefore, working out how to accurately estimate the transmission map and reduce the noise pollution are the key steps to restore images.

The high quality of a snow-free image depends on the accurate estimation of parameters. In this paper, we propose an efficient physical scheme (polarimetric information), which can accurately estimate the parameters (infinity airlight and transmission map) of the atmospheric physical scattering model. Then, the snow-free image has been inversed by the atmospheric physical scattering model. This method does not rely on the sky region and can be used for nonsky images, even those not affected by a higher brightness scene. This method implements a simple formula and has higher computational efficiency. First, we take four polarimetric images

at different orientations to obtain the degree of polarization (DOP) and the angle of polarization (AOP) by the Stokes vector. Second, airlight at infinity is estimated by the maximum value of the DOP and AOP; then through the airlight at infinity, the global transmission map is acquired. Finally, based on the atmospheric scattering model, the image is recovered. Experimental results show that this technique can improve the image quality, reconstruct the original color, and recognize more details, especially for enhancing visibility and increasing contrast.

2. Principal

2.1. Atmospheric scattering model

In our scheme, the atmospheric scattering model is used to restore the image under snowy weather conditions. The physical model has been widely used in image processing [1–3, 17], and the mathematical formula of the model can be expressed as follows:

$$I(x, y) = L(x, y) \cdot t(x, y) + A_\infty [1 - t(x, y)], \qquad (1)$$

where $I(x, y)$ is the total intensity received by the device, and is radiance of the scene without attenuate, which is the major goal that we need to recover; $L(x, y)$ is the transmission function, the degraded image is in an exponential decay, so $t(x, y)$ can be expressed as $t(x, y) = \exp(-\beta d)$, β is the scattering coefficient of the atmosphere and it can be regarded as a constant in the homogeneous atmosphere condition, and is the radiance distance from scene to device. The term $L(x, y) \cdot t(x, y)$ denotes the direct light, which describes the object's radiance and attenuation in the medium; $A_\infty [1 - t(x, y)]$ denotes the airlight [14].

From equation (1), the recovered image can be expressed as:

$$L(x, y) = \frac{I(x, y) - A_\infty [1 - t(x, y)]}{t(x, y)}. \qquad (2)$$

From equation (2), we can find that the transmission map $t(x, y)$ and atmospheric airlight at infinity A_∞ are the key parameters to reconstruct the image. Therefore, we used the scheme of the Stokes vector to estimate the optimal of these two parameters as follows.

2.2. $t(x, y)$ and A_∞ estimation

Through the polarization state of the polarimetric image, we estimated the transmission map $t(x, y)$ and atmospheric airlight at infinity A_∞. The polarization state can be represented by the Stokes vector [25]. Therefore, we place a linear polarizer in front of the camera, and we define any starting location as $0°$. Then, we rotate the polarizer in sequence to three orientations of $45°$, $90°$, and $135°$, and thus different intensities of the four images at different orientations are acquired. The intensities of the polarimetric images at orientations of $0°$, $45°$, $90°$, and $135°$ can be represented as $I_0(x, y)$, $I_{45}(x, y)$, $I_{90}(x, y)$, and $I_{135}(x, y)$, respectively. The

Stokes vector of incident light can be expressed as:

$$\begin{bmatrix} S_0(x, y) \\ S_1(x, y) \\ S_2(x, y) \end{bmatrix} = \begin{bmatrix} I_0(x, y) + I_{90}(x, y) \\ I_0(x, y) - I_{90}(x, y) \\ I_{45}(x, y) - I_{135}x, y) \end{bmatrix} \quad (3)$$

where $S_0(x, y)$ represents the total intensity of light; $S_1(x, y)$ represents the amount of linear horizontal or vertical polarization; $S_2(x, y)$ represents the amount of $+45°$ or $-45°$ polarization; we neglect circular-polarized light because its component is sufficiently small in the atmosphere. Based on equation (3), we can obtain (DOP, ρ) and (AOP, θ); they can be expressed as:

$$\rho(x, y) \underset{c \in \{R,G,B\}}{=} \frac{\sqrt{(S_1^c(x, y))^2 + (S_2^c(x, y))^2}}{S_0^c(x, y)}, \quad (4)$$

$$\theta(x, y) \underset{c \in \{R,G,B\}}{=} \frac{1}{2} \arctan \frac{S_2^c(x, y)}{S_1^c(x, y)} \quad (5)$$

where $c \in \{R, G, B\}$ represents RGB space per-patch. We calculate the ρ and θ in the RGB color channels per pixel.

In order to obtain a high-quality restored image, precise estimation of the transmission map $t(x, y)$ and atmospheric airlight A_∞ at infinity is very important. Generally, polarization-based methods select the highest luminance value of the sky region to estimate A_∞ [18], and this scenario makes color artificialness of the sky region. Therefore, the scheme we proposed is not limited by the sky region and is not affected by a higher brightness object. Our scheme adopts the scenario of mathematical statistics to obtain the maximum value of ρ and θ by global analysis (first, we calculate AOP and DOP in the RGB channel. The we calculate the average of the RGB channel in each pixel, and acquire the maximum AOP and DOP) to estimate A_∞. In the next formulas, the maximum values of ρ and θ can be expressed as ρ_m and θ_m, respectively. From equation (1), the radiance distance d can be approximately regarded as infinity; thus, the total intensity $I(x, y)$ is approximately equal to A_∞. In fact, $L(x, y) \cdot t(x, y)$ is finally depolarized, and A_∞ is partially polarized airlight. Based on reference [26], double $I(0)$ is difficult to represent the total intensity; this leads to underestimation of A_∞, so we impose the Stokes vector ($I(0)$ and $I(90)$) to represent the total intensity, and A_∞ can be defined as:

$$A_\infty(x, y) \underset{c \in \{R,G,B\}}{=} \frac{S_0(x, y)^c}{1 + \rho_m \cos 2\theta_m}. \quad (6)$$

In equation (6), $S_0(x, y)^c = I(0) + I(90)$ is the total intensity in the RGB space channel. Subsequently, we estimate the transmission map. The transmission map $t(x, y)$ is the medium transmission describing the portion of light, which is received by the detector. The atmospheric airlight at infinity A_∞ is the value of airlight at a nonblurred horizon [22]. Due to the polarization state of light reflected from scenes being regarded as zero, then θ_m can be expressed as the AOP of the airlight. Moreover the $0°$ and $90°$ polarized light are orthogonal in coordinate system, and θ_m is in the range of $0°$ to $90°$ [27]. Therefore, we can assume that the atmospheric airlight at infinity A_∞ includes part of the information about the light, so based on the orthotropic coordinate, the
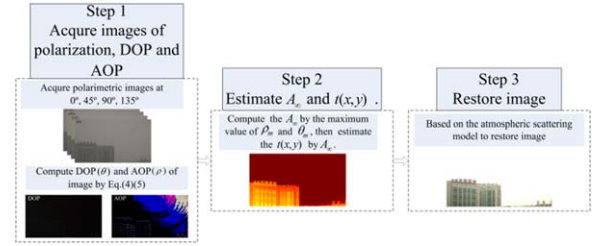

Figure 1. Flowchart of our method.

transmission map $t(x, y)$ can be represented as the atmospheric airlight at infinity in the θ_m direction. Then $t(x, y)$ can be expressed as:

$$t(x, y) = A_\infty(x, y) \cdot \cos \theta_m. \quad (7)$$

Because snowflakes affect the transmission map and decrease the quality of the processed image, we consider that snowflakes are a type of noise. Therefore, in order to obtain smooth $t(x, y)$ in a local area, it is necessary to filter and denoise the transmission map $t(x, y)$. We adopt the method of weighted average in the three color channels to avoid this issue. In addition, the global analysis scenario can estimate A_∞ more conveniently and precisely. The atmospheric light at infinity A_∞ and the transmission map $t(x, y)$ are based on the approach of statistics; therefore, this method can provide a simple formula and low computational cost.

2.3. Overview

We present a new approach, which is based on ρ_m and θ_m to estimate A_∞ and $t(x, y)$. The flowchart of our method is shown in figure 1. This method mainly includes three steps: the first step aims at acquiring the image of the DOP and AOP based on polarimetric images at four orientations. In the second step, we used the scheme of the global analysis to obtain the maximum values of ρ and θ of the image of the DOP and AOP, respectively. Then we used the ρ_m and θ_m to compute the airlight at infinity. Subsequently, we used the A_∞ to estimate the transmission map $t(x, y)$. Because the noise (snowflakes) of the transmission map $t(x, y)$ affects the quality of the restored image, we utilized the weighted average in the three color channels to eliminate the noise. In the final step, we acquired the recovered image based on the atmospheric scattering model.

3. Experiments and result

In our experiments, we rotated the linear polarizer in front of the device and acquired images. We need to keep the device stabilized, otherwise the different-orientation images will malposition, which will lead to ghost images and affect the final quality of the restored images. As shown in figure 2, there are three typical groups of images at four orientations ($0°$, $45°$, $90°$, and $135°$). We acquired these images under the atmospheric condition of snow in the afternoon (the pixel number of each image is 1920×1080). The main scenes of the images are buildings and plaques; these scenes can
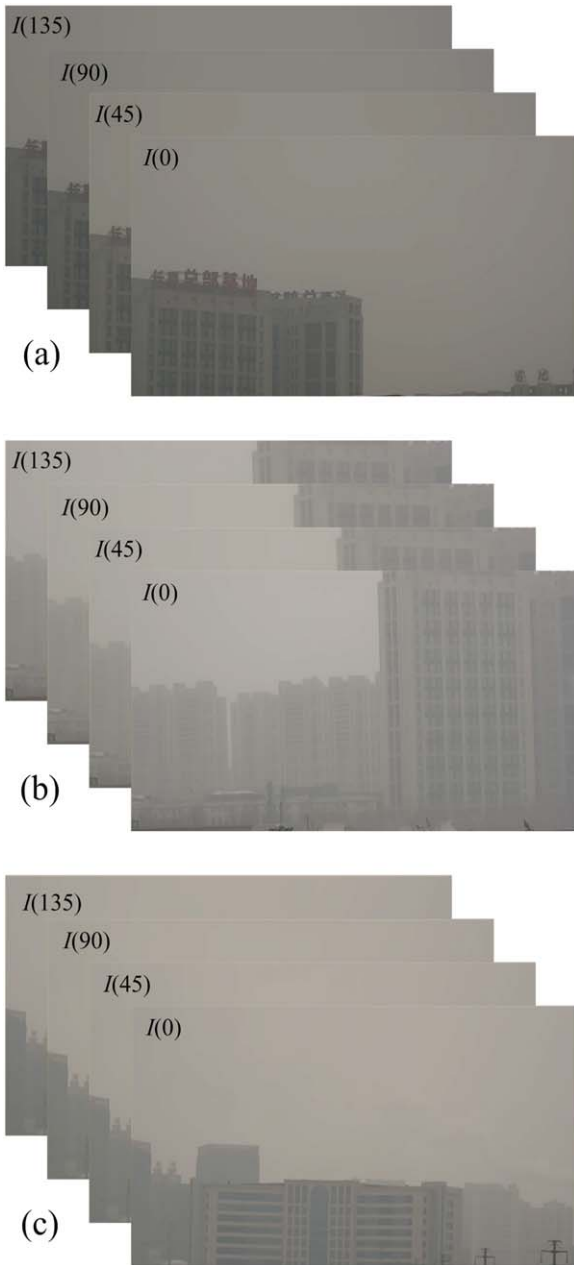
Figure 2. Three groups of snowy images with different scenes at 0°, 45°, 90°, and 135° orientations.
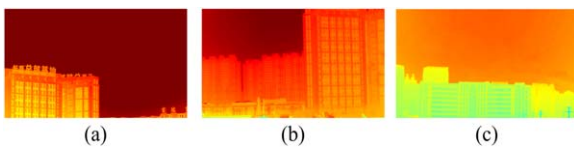

Figure 3. Transmission map of three snow images.

significantly demonstrate whether our method enhances visibility and recovers the real colors.

Next, we process images by the method that we proposed. Through the polarimetric images, we obtain the Stokes vector and calculate the DOP and AOP by the Stokes vector. Subsequently, we count the maximum values of ρ and θ to estimate A_∞, then estimate the transmission map $t(x, y)$,
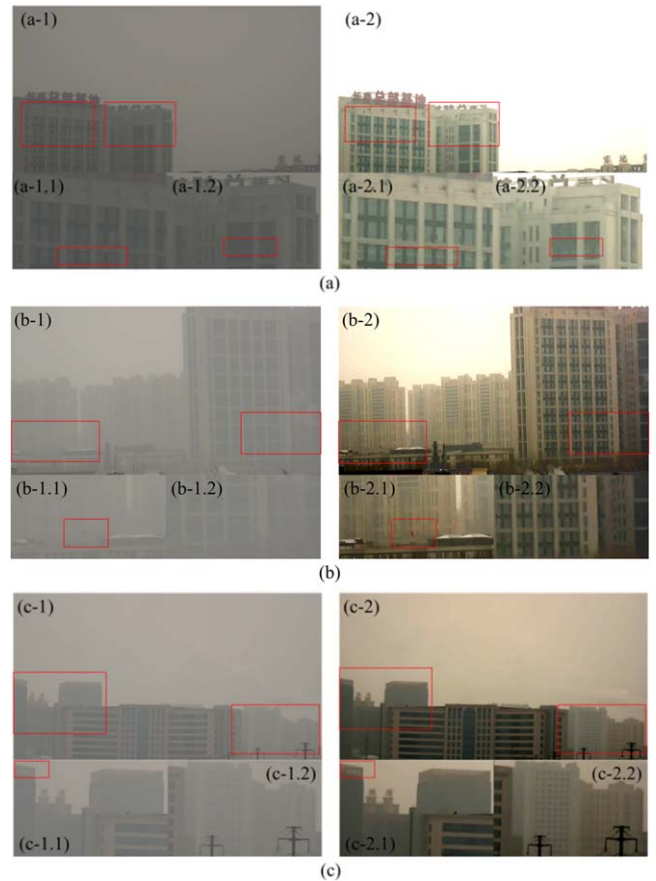

Figure 4. Three original images and their corresponding restored images. (a-1), (b-1), and (c-1) are the original images, (a-2), (b-2), and (c-2) are the restored images; below the original and restored images are the magnified images of details in the red rectangle region of the original and restored images.

which is shown in figure 3. From figure 3, we can find that the transmission map $t(x, y)$ can divide the scene and the sky region obviously and make the outline of the scenes easily distinguishable. We adopt the method of the weighted average, which can eliminate the noise and avoid the detailed information from being submerged into the noise, which is caused by snowflakes. Therefore, the quality of the processed images depends on the precise estimation of the transmission map.

Based on the transmission map $t(x, y)$ and the atmospheric scattering model, we restored the blurred images. Figure 4 shows the contrast of the original images with the restored images in detail. From figures 4(a)–(c), we observe that the original image quality is affected by snowy weather, so they lost their color fidelity and the outline of the buildings is difficult to recognize. Meanwhile, we can find that our method can significantly improve visibility and correct the color shift. In figures 4(a-2), (b-2), and (c-2), the buildings recover sharp edges and the real color, the color of the plaque is restored naturally, and the characters of the plaque can be recognized easily. We compared the red rectangle region in figure 4(a-1) and (a-2); images of (a-1.1), (a-1.2), (a-2.1), and (a-2.2) are the magnified images of this region. In figure 4(a-1.1) and (a-2.1), the red rectangular region shows that the recovered
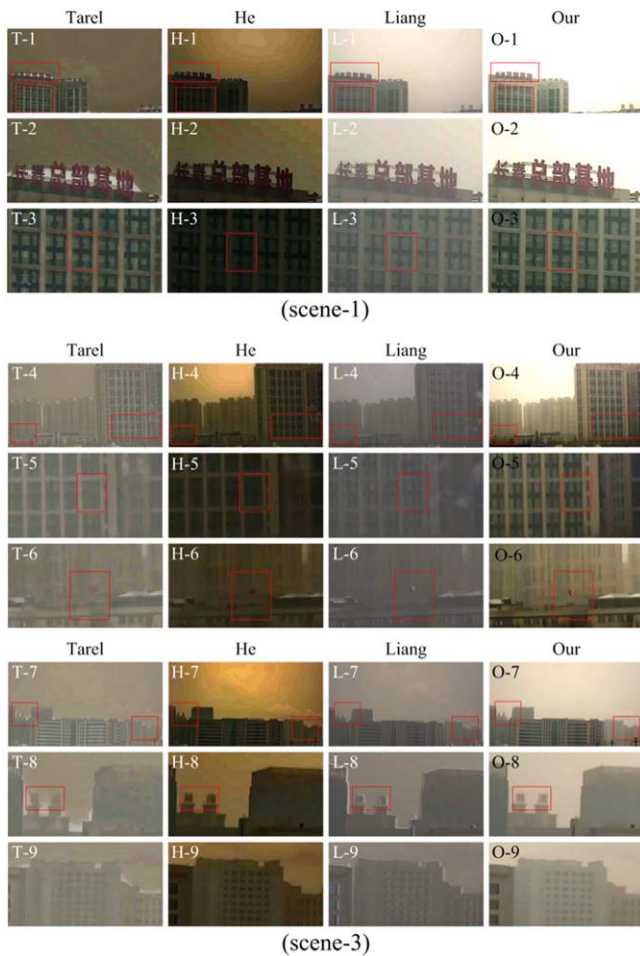
Figure 5. The performance of different methods with enlarged details.

image includes more detailed information. In figures 4(b-1.2) and (b-2.2), it is difficult to distinguish the outline of the windows in the original image, but the restored image captures the sharp edge discontinuities and outlines the profile of the buildings. Especially in the red rectangular region of figures 4(b-1.1) and (b-2.1), we can see that the recovered image has a red flag, which is difficult to observe in the original image. We compared figures 4(c-1.1) with figure 4(c-2.1) in the red rectangular region. This method can significantly reconstruct the characteristics of the plaque, which means that this method can enhance visibility. Besides, in figures 4(c-1.2) and (c-2.2), the reconstructed image has much better performance than the original image; particularly, the windows' profile of further buildings can be more easily distinguished in figure 4(c-1.2) than in figure 4(c-2.2).

Next, we compared the typical methods of Tarel [28], He [15] and Liang [26] with our method. The methods of Tarel and He are typical computer vision methods, and Liang's method is based on the polarimetric method. We keep the intrinsic parameters of the source code. The removal results and the enlarged details' performance are demonstrated in figure 5. In figure 5, the results of Tarel and He have been overcorrected, moreover, their results introduce unpleasing artifacts in the sky region. The results of Liang perform better than Tarel and He, but in figure 5(L-3), the color results in an

unnatural transition in the sky and object regions. We enlarge the details of the red rectangular regions and compare with the abovementioned methods. The results of Tarel's method has an unnatural color in the plaque and sky regions (e.g. T-1.1, T-3.1, T-3.2), even the recovered images have a reduced resolution (e.g. T-2.1, T-2.2, T-3.1, T-3.2), which cannot preserve more detail. Moreover, the methods of Tarel and Liang produce results with a halo in the sharp edges (e.g. in T-1.1, T-3.1, L-3.1, L-3.2), meanwhile, the recovered images with server noise include outlines of the windows that are difficult to distinguish. The color of Liang's result has low saturation, it is hard to distinguish the red flag in figure 5(L-2.2), but in figure 5(O-2.2), the red flag is more easily detected by our method.

Comparing the methods shows that Tarel's method can unveil and remove the blur slightly, but the recovered images have faded color. Tarel's method is based on a median filter, which cannot accurately estimate the transmission map. Moreover, there is a halo in the discontinuous areas, especially in the adjacent area between the sky and objects. The results of He's method show better performance than Tarel's method, but the color of the recovered images has been overcorrected. He's method depends on the validity of the prior dark channel, one may fail when the object is brighter than atmospheric light. Liang's method is based on polarimetric information to estimate the airlight. We observed that the recovered images with severe noise will degrade the image quality. In our experience, we find that estimating the polarized part of airlight will be invalid when the AOP of airlight is $0°$ or $90°$. Moreover, estimating the matrix of DOP will be invalid, when the most frequently appearing value of AOP is $45°$. In contrast, our method not only corrects color fidelity and recovers details, but also enhances visibility. Moreover, our method is more suitable to human visual characteristics by contrast results.

In order to evaluate our method in an objective manner, we used the noreference image quality to assess the quality of our method, which is the nature image quality evaluator (NIQE) [29] and the ratio between the gradient of the visible edges between the image before and after contrast restoration [30]. The NIQE assesses the normal luminance coefficients of a nature image. The normal luminance coefficients follow the Gaussian distribution, but the hazy image is always against this distribution. In reference [30], the method of assessing the image quality is based on e, r and σ, which represent the ratio of the newly visible edge, the normalized gradient mean value of the visible edge, and the percentage of the saturated black or white pixel point, respectively. Higher values of e and r, or a low value of σ indicate higher image quality. The mean score of each method for three different scenes is listed in table 1.

From table 1, we can see that our method has the highest performance in terms of the NIQE, σ and r, so it can be demonstrated that our method has the advantage of enhancing visibility and restoring images. In addition, figure 6 shows the distribution of the RGB color components in each pixel of the restored images. The comparison results illustrate that these methods can enhance the color range of the blurred image. In
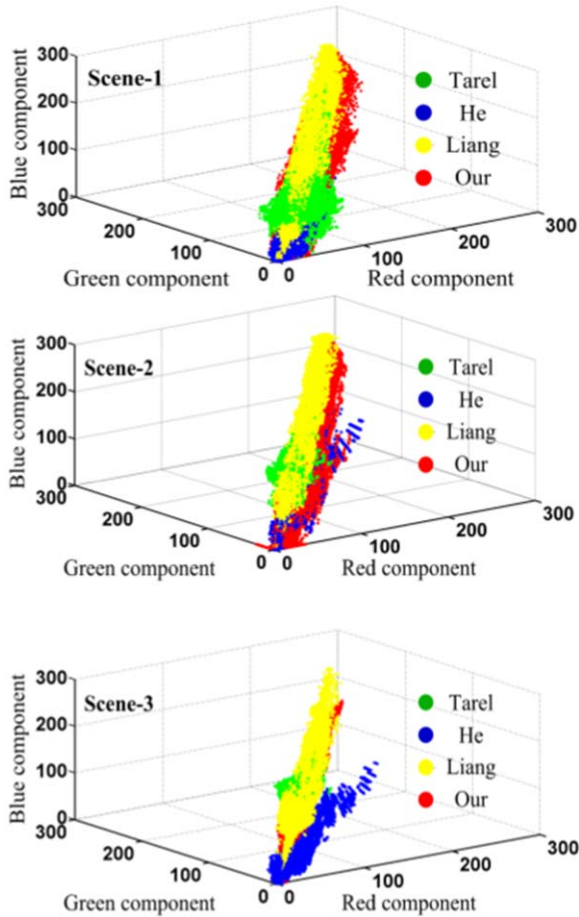
Figure 6. Distributions of the RGB color components. The green dots represent Tarel's method, the blue dots represent He's method, the yellow dots represent Liang's method and the red dots represent our method.

Table 1. Quantitative comparison of these methods for various performance indices.

	NIQE	e	σ	r
Tarel	7.0356	5.5983	0.0246%	3.7736
He	6.1179	**15.229**	0.0172%	2.1468
Liang	7.4476	6.9899	0.0067%	3.0774
Our	**8.4340**	8.5753	**0.0019%**	**4.0668**

scene-1 and scene-2, our method has the largest range of colors than the other methods. In scene-2 and scene-3, we can observed that He's results have a larger range than our method in the R-channel, but He's results have a lower RGB range, and the distribution of RGB is nonuniform distribution; this demonstrates that the color of the recovered image is incorrect (the recovered image with over-saturated colors). In scene-3, our method and Liang's method have a similar performance in the RGB component, but in scene-1 and scene-2, our results are better than Liang's. From the results of the RGB component, the RGB component of the recovered image is uniformly distributed by our method. Moreover, our

Table 2. Time consumption of different methods.

Image resolution	Tarel's	He's	Liang	Our
1920 × 1080(Scene-1)	353.486 s	7.514 s	7.976 s	3.083 s
1920 × 1080(Scene-2)	368.560 s	7.539 s	8.073 s	3.582 s
1920 × 1080(Scene-3)	362.424 s	7.449 s	8.069 s	3.815 s

method can correct the color shift and increase the visibility moderately.

In addition, our method was compared with Tarel's method, He's method and Liang's method in terms of the computational cost, as can be seen in table 2. The image resolution of the three typical scenes is 1920 × 1080, and we used the Matlab 2016b package, which runs on an Intel(R) Core(TM) 4.00-GHz CPU with 8 GB of RAM to compute processing times. Our method has a lower computational cost than the other three methods. Therefore, our method has higher efficiency. If we adopt an aperture-division polarimetric camera to acquire images (this device can acquire images at four orientations simultaneously and has lower resolution), the computational cost should be decreased significantly and our method can be used to process real-time images.

4. Conclusion

In this paper, we proposed a polarization-based method to restore images in snowy weather. Because the characteristics of snow are dynamic, it is difficult to estimate morphological features and establish the corresponding physical model. In our method, snowflakes are considered as noise, and the transmission map is reconstructed to restore the image. Thus, with our method, it is possible to handle this issue under real environmental conditions of snowy weather. Experimental results in this study allow us to assess the advantages of using the polarization-based method to enhance visibility and correct the color shift. It can be concluded that our method has a simple formula to reconstruct blurred images, and the results demonstrate a significant improvement in the contrast and restore detailed information. Moreover, our method can avoid unfaithful estimation of the transmission map caused by susceptible bright objects or strong light sources. Moreover, the results have shown that the sky region of the restored image has no significant depolarized halo through snowy weather over a kilometer, and this method is independent of prior knowledge at a kilometric distance. Therefore, our method has advantages of enhancing visibility of such degraded images. Furthermore, our method has a low computational cost for high-resolution images.

In summary, we presented a simple polarization-based scheme to estimate the transmission map more accurately. Compared to the previously proposed methods, our method can obtain a high-quality image in snowy weather at a long range. Moreover, as our method is polarization-based, which is required to acquire images at four orientations, the camera

platform should be stabilized, which prevents the images from mismatch happening. In order to avoid ghost imaging and capture real-time unveiled images, we will use an aperture-division polarimetric camera in the future.

Acknowledgments

ORCID iDs

YongNan Lu ⓘ https://orcid.org/0000-0002-2191-2493

References

[1] Garg K and Nayar S K 2007 Vision and rain *Int. J. Comput. Vis.* **75** 3–27

[2] Chitwood D, Henry R C, Urquijo S and Mahadev S 2000 Color perception through atmospheric haze *J. Opt. Soc. Am.* A **17** 831–5

[3] Narasimhan S G and Nayar S K 2002 Vision and the atmosphere *Int. J. Comput. Vis.* **48** 233–54

[4] Narasimhan S G and Nayar S K 2003 Contrast restoration of weather degraded images *IEEE Trans. Pattern Anal. Mach. Intell.* **25** 713–24

[5] Li X, Hu H, Zhao L, Wang H, Yu Y, Wu L and Liu T 2018 Polarimetric image recovery method combining histogram stretching for underwater imaging *Sci. Rep.* **8** 12430

[6] Tian H, Zhu J, Tan S, Zhang Y, Zhang Y, Li Y and Hou X 2018 Rapid underwater target enhancement method based on polarimetric imaging *Opt. Laser Technol.* **108** 515–20

[7] Hase H, Miyake K and Yoneda M 2002 Real-time snowfall noise elimination *Int. Conf. on Image Processing* vol 2 2002 pp 406–9

[8] Fu Y H, Kang L W, Lin C W and Hsu C T 2011 Single-frame-based rain removal via image decomposition *IEEE Int. Conf. on Acoustics, Speech and Signal Processing* **2011** 178–86

[9] Ding X, Chen L, Zheng X, Huang Y and Zeng D 2016 Single image rain and snow removal via guided L0 smoothing filter *Multimed. Tools Appl* **75** 2697–712

[10] Rajderkar D and Mohod P S 2013 Removing snow from an image via image decomposition *Int. Conf. on Emerging Trends in Computing, Communication and Nanotechnology* **2013** 576–9

[11] Liu S, Rahman M A, Liu S C, Wong C Y, Lin C F and Wu H 2017 Image de-hazing from the perspective of noise filtering *Comput. Electr. Eng.* **62** 345–59

[12] Fattal R 2008 Single image dehazing *ACM Trans. Graph.* **27** 1–9

[13] Barnum P C, Narasimhan S and Kanade T 2010 Analysis of rain and snow in frequency space *Int. J. Comput. Vis.* **86** 256

[14] Tan R T 2008 Visibility in bad weather from a single image *IEEE Proc. Conf. on Computer Vision and Pattern Recognition* pp 1–8

[15] He K, Sun J and Tang X 2011 Single image haze removal using dark channel prior *IEEE Trans. Pattern Anal. Mach. Intell.* **33** 2341–53

[16] Zhu Q, Mai J and Shao L 2015 A fast single image haze removal algorithm using color attenuation prior *IEEE Trans. Image Processing* **24** 3522–33

[17] Schechner Y Y, Narasimhan S G and Nayar S K 2003 Polarization-based vision through haze *Appl. Opt.* **42** 511–25

[18] Schaul L, Fredembach C and Süsstrunk S 2010 Color image dehazing using the near-infrared *IEEE Int. Conf. on Image Processing* pp 1629–32

[19] Feng C, Zhuo S, Zhang X, Shen L and Susstrunk S 2014 Near-infrared guided color image dehazing *IEEE Int. Conf. on Image Processing* pp 2363–7

[20] Liang J, Zhang W, Ren L, Ju H and Qu E 2016 Polarimetric dehazing method for visibility improvement based on visible and infrared image fusion *Appl. Opt.* **55.29** 8221–6

[21] Liu F, Cao L, Shao X, Han P and Bin X 2015 Polarimetric dehazing utilizing spatial frequency segregation of images *Appl. Opt.* **54** 8116–22

[22] Namer E, Shwartz S and Schechner Y Y 2009 Skyless polarimetric calibration and visibility enhancement *Opt. Express* **17** 472

[23] Fang S, Xia X, Xing H and Chen C 2014 Image dehazing using polarization effects of objects and airlight *Opt. Express* **22** 19523–37

[24] Qu Y and Zou Z 2017 Non-sky polarization-based dehazing algorithm for non-specular objects using polarization difference and global scene feature *Opt. Express* **25** 25004

[25] Bass M, Stryland E W V, Williams D R and Wolfe W L 1995 *Handbook of Optics Volume II Devices, Measurements, and Properties* 2nd edn (New York: McGraw-Hill)

[26] Liang J, Ren L Y, Ju H J, Qu E S and Wang Y L 2014 Visibility enhancement of hazy images based on a universal polarimetric imaging method *J. Appl. Phys.* **116** 173107

[27] Zhang W, Liang J, Ren L, Ju H, Bai Z and Wu Z 2017 Fast polarimetric dehazing method for visibility enhancement in HSI colour space *J. Opt.* **19** 095606

[28] Tarel J P and Hautière N 2010 Fast visibility restoration from a single color or gray level image *IEEE Int. J. Comput. Vis.* pp 2201–8

[29] Mittal A, Soundararajan R and Bovik A C 2013 Making a 'completely blind' image quality analyzer *IEEE Signal Proc. Let.* **20** 209–12

[30] Hautière N, Tarel J P, Aubert D and Dumont É 2011 Blind contrast enhancement assessment by gradient ratioing at visible edges *Image Anal. Stereol.* **27** 87–95